# Inclusive Quasi-Elastic Neutrino Reactions

Juan NIEVES
*Departamento de Física Moderna, Universidad de Granada, Campus de Fuentenueva, S/N, E-18071 Granada, Spain*
José Enrique AMARO
*Departamento de Física Moderna, Universidad de Granada, Campus de Fuentenueva, S/N, 18071 Granada, Spain*
Manuel VALVERDE
*Departamento de Física Moderna, Universidad de Granada, Campus de Fuentenueva, S/N, 18071 Granada, Spain*
Eulogio OSET
*Departamento de Física Teórica and IFIC, Centro Mixto Universidad de Valencia-CSIC, 46100 Burjassot (Valencia), Spain*

**Abstract**

The Quasi-Elastic (QE) contribution of the nuclear inclusive electron scattering model developed in [1] is extended to the study of electroweak Charged Current (CC) induced nuclear reactions, at intermediate energies of interest for future neutrino oscillation experiments. The model accounts for long range nuclear (RPA) correlations, Final State Interaction (FSI) and Coulomb corrections. RPA correlations are shown to play a crucial role in the whole range of neutrino energies, up to 500 MeV, studied in this work. Predictions for inclusive muon capture for different nuclei, and for the reactions $^{12}\mathrm{C}(\nu_\mu, \mu^-)X$ and $^{12}\mathrm{C}(\nu_e, e^-)X$ near threshold are also given.

## 1. Introduction

Neutrino properties have been object of much interest as long as they could provide hints of physics beyond the standard model. A sensitive way to study the mass of the neutrino is by means of neutrino oscillations. One of the various experiments devoted to this topic is the atmospheric neutrinos detection carried out in Kamiokande and Superkamionde, which data have given evidence on $\nu_\mu \to \nu_\tau$ oscillation with $10^{-3} \lesssim \Delta m^2 \lesssim 10^{-2}$ and almost maximal mixing angle, see [2] for a review. Once this phenomena have been firmly stablished new questions arise, such as the role of three flavour oscillations and the precise

pp. 165–181 

determination of the values of neutrino masses and mixing parameters [3]. For the obtention of accurate results in these new experiments it is necessary to keep under control the sources of systematic error. Two of the major sources of systematic errors in the sub-GeV samples of SK experiments are the charged and neutral-current cross sections [4]. Thus, if we want to cope with the requirements of this new experiments precise nuclear interaction models must be used.

Any model aiming at describing the interaction of neutrinos with nuclei should be firstly tested against the existing data on the interaction of real and virtual photons with nuclei. At intermediate energies (nuclear excitation energies ranging from about 100 MeV to 500 or 600 MeV) three different contributions should be taken into account: i) Quasi-Elastic (QE) processes, ii) pion production and two body processes from the QE region to that beyond the $\Delta(1232)$ resonance peak, and iii) double pion production and higher nucleon resonance degrees of freedom induced processes. The model developed in [1] (inclusive electro–nuclear reactions) and [5] (inclusive photo–nuclear reactions) has been successfully compared with data at intermediate energies and it systematically includes the three type of contributions mentioned above. The building blocks of this model are: i) a gauge invariant model for the interaction of real and virtual photons with nucleons, mesons and nucleon resonances with parameters determined from the vacuum data, and ii) a microscopic treatment of nuclear effects, including long and short range nuclear correlations [6], FSI, explicit meson and $\Delta(1232)$ degrees of freedom, two and three nucleon absorption channels, etc. Finite size effects are computed from a Local Fermi Gas (LFG) picture of the nucleus, which is an accurate approximation to deal with inclusive processes which explore the whole nuclear volume [5]. The parameters of the model are completely fixed from previous hadron-nucleus studies: pionic atoms, elastic and inelastic pion-nucleus reactions, $\Lambda-$hypernuclei, etc. [7]. The photon coupling constants are also determined in the vacuum. Thus the model of [1] and [5] has no free parameters, and hence these results are predictions deduced from the nuclear microscopic framework developed in [6] and [7]. In this talk, we show an extension of the nuclear inclusive QE electron scattering model of [1], including the axial CC current, to describe neutrino and antineutrino induced nuclear reactions in the QE region. We will not show here many details of the model, for a detailed discussion we refer the reader to [8].

## 2. Inclusive cross section

We will present here the general formalism focusing on the neutrino Charged-Current (CC) reaction

$$\nu_l(k) + A_Z \rightarrow l^-(k') + X \tag{1}$$

though the generalization of the obtained expressions to antineutrino induced reactions or inclusive muon capture in nuclei is straightforward.

The double differential cross section, with respect to the outgoing lepton kinematical variables, for the process of Eq. (1) is given in the Laboratory (LAB) frame by

$$\frac{d^2\sigma_{\nu l}}{d\Omega(\hat{k'})dE'_l} = \frac{|\vec{k'}|}{|\vec{k}\ |}\frac{G^2}{4\pi^2}L_{\mu\sigma}W^{\mu\sigma} \tag{2}$$

with $L$ and $W$ the leptonic and hadronic tensors, respectively.

The hadronic tensor $W^{\mu\nu}$ includes non-leptonic vertices and corresponds to the charged electroweak transitions of the target nucleus to all possible final states; it is completely determined by six independent, real Lorentz scalar structure functions $W_i(q^2)$ , $i = 1, \ldots, 6$.

We follow here the formalism of [1], and evaluate the self-energy $\Sigma^r_\nu(k;\rho)$ of a neutrino with helicity $r$ inside of a nuclear medium of density $\rho$. Diagrammatically this is depicted in Fig. 1. After summing over helicities, we get

$$\Sigma_\nu(k;\rho) = \frac{8\mathrm{i}G}{\sqrt{2}M_W^2}\int\frac{d^4q}{(2\pi)^4}\frac{L_{\eta\mu}\Pi_W^{\mu\eta}(q;\rho)}{k'^2 - m_l^2 + \mathrm{i}\epsilon} \tag{3}$$

where $\Pi_W^{\mu\rho}(q)$ is the $W^+-$boson self-energy in the nuclear medium.

The neutrino disappears from the elastic flux, by inducing one particle - one hole (1p1h), 2p2h ... excitations, $\Delta(1232)-$hole ($\Delta$h) excitations, or creating pions, etc...at a rate given by

$$\Gamma(k;\rho) = -\frac{1}{k^0}\mathrm{Im}\Sigma_\nu(k;\rho) \tag{4}$$

To evaluate the imaginary part of $\Sigma_\nu$ we use the Cutkosky's rules, and we cut with a straight vertical line (see Fig. 1) the intermediate lepton state and those produced by the $W-$boson polarization (shaded region). Those states are then placed on shell by taking the imaginary part of the propagator, self-energy, etc. Thus, we obtain

$$\mathrm{Im}\Sigma_\nu(k) = \frac{8G}{\sqrt{2}M_W^2}\int\frac{d^3k'}{(2\pi)^3}\frac{\Theta(q^0)}{2E'_l}\mathrm{Im}\left\{\Pi_W^{\mu\eta}(q;\rho)L_{\eta\mu}\right\} \tag{5}$$

for $k^0 > 0$.

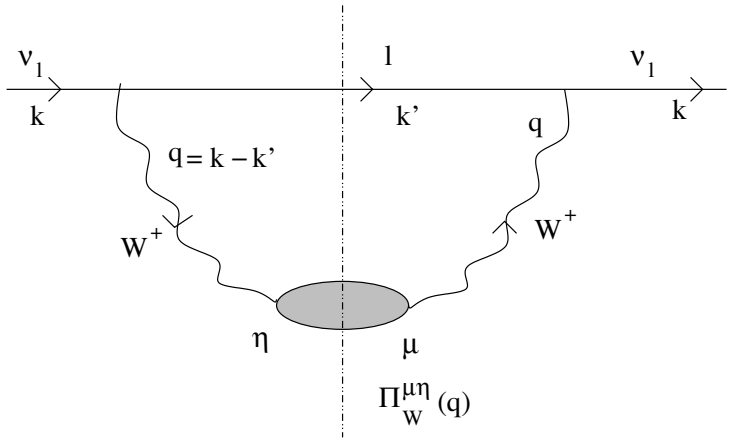


**Fig 1.** Diagrammatic representation of the neutrino self-energy in nuclear matter.

Since $\Gamma dtdS$ provides a probability times a differential of area, which is a contribution to the $(\nu_l, l^-)$ cross section, we have

$$d\sigma = \Gamma(k;\rho)dtdS = -\frac{1}{k^0}\mathrm{Im}\Sigma_\nu(k;\rho)dtdS = -\frac{1}{|\vec{k}|}\mathrm{Im}\Sigma_\nu(k;\rho)d^3r \qquad (6)$$

so the nuclear cross section is given by

$$\sigma = -\frac{1}{|\vec{k}|}\int \mathrm{Im}\Sigma_\nu(k;\rho(r))d^3r \qquad (7)$$

where we are considering $\Sigma_\nu$ a function of the nuclear density $\rho(r)$ at each point of the nucleus and we integrate over the whole nuclear volume. We assume LDA, which, as shown in [5], is an excellent approximation for volume processes like the one studied here. Coming back to Eq. (7) we can compare it with Eq. (2) so the hadronic tensor ($W^{\mu\sigma} = W_s^{\mu\sigma} + iW_a^{\mu\sigma}$) reads

$$W_s^{\mu\sigma} = -\Theta(q^0)\left(\frac{2\sqrt{2}}{g}\right)^2 \int \frac{d^3r}{2\pi}\ \mathrm{Im}\left[\Pi_W^{\mu\sigma} + \Pi_W^{\sigma\mu}\right](q;\rho) \qquad (8)$$

$$W_a^{\mu\sigma} = -\Theta(q^0)\left(\frac{2\sqrt{2}}{g}\right)^2 \int \frac{d^3r}{2\pi}\ \mathrm{Re}\left[\Pi_W^{\mu\sigma} - \Pi_W^{\sigma\mu}\right](q;\rho) \qquad (9)$$

from where we can see how $\Pi_W^{\mu\sigma}$ is the basic object of our approach. Following the lines of [1], we should perform a many body expansion, where the relevant gauge-boson absorption modes would be systematically incorporated: absorption by one, two or even three nucleon mechanisms, real and virtual meson ($\pi$, $\rho$, $\cdots$) production, excitation of $\Delta$ or higher resonance degrees of freedom, etc. Some of these modes are depicted in Fig. 2.

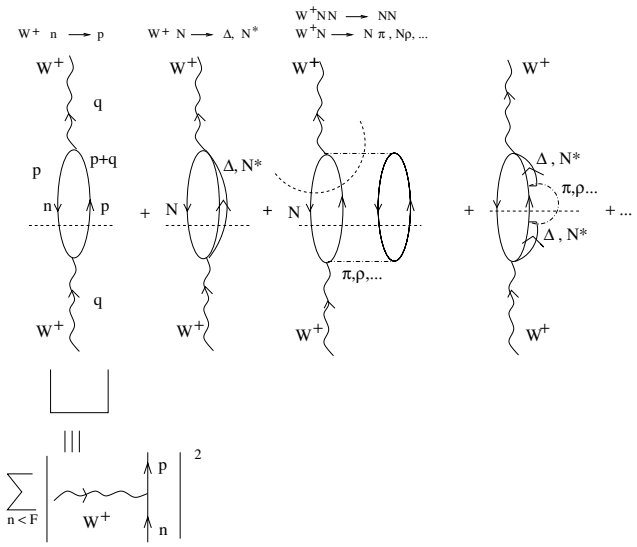


**Fig 2.** Diagrams of some processes contributing to the $W^+$ self-energy.

## 3. QE contribution to $\Pi^{\mu\sigma}_W$

The virtual $W^+$ can be absorbed by one nucleon leading to the QE contribution of the nuclear response function. Such a contribution corresponds to a 1p1h nuclear excitation (first of the diagrams depicted in Fig. 2). We will work on a non-symmetric nuclear matter with different Fermi sea levels for protons than for neutrons. For the $W^+$-$pn$ vertex we consider the $V-A$ current, and use PCAC and invariance under G-parity to relate the pseudoscalar form factor to the axial one and to discard a term of the form $(p^\mu + p'^\mu)\gamma_5$ in the axial sector, respectively. Invariance under time reversal guarantees that all form factors are real. Using isospin symmetry we can relate the vector form factors with the electromagnetic ones.

With all of these ingredients is straightforward to evaluate the contribution to the $W^+$ self-energy of the first diagram of Fig. 2. We finally get

$$W^{\mu\nu}(q^0,\vec{q}) = -\frac{\cos^2\theta_C}{2M^2}\int_0^\infty dr r^2 2\Theta(q^0)\int\frac{d^3p}{(2\pi)^3}\frac{M}{E_{\vec{p}}}\frac{M}{E_{\vec{p}+\vec{q}}}(-\pi)$$
$$\times\,\Theta(k_F^n-|\vec{p}\,|)\Theta(|\vec{p}+\vec{q}\,|-k_F^p)\delta(q^0+E_{\vec{p}}-E_{\vec{p}+\vec{q}})A^{\nu\mu}(p,q)|_{p^0=E_{\vec{p}}} \tag{10}$$

with the CC nucleon tensor $A^{\mu\nu}$ obtained after taking some traces on the Dirac's space. The $d^3p$ integrations above can be done analytically and all of them are determined by the imaginary part of the relativistic isospin asymmetric Lindhard function, $\overline{U}_R(q,k_F^n,k_F^p)$. Explicit expressions for $\overline{U}_R$ and $A^{\mu\nu}$ are given in [8].

Up to this point the treatment is fully relativistic. To account for RPA effects, we will use a nucleon–nucleon effective force, so for consistency we ought to use a non-relativistic Fermi gas. This is easily done by replacing the factors $M/E_{\vec{p}}$ and $M/E_{\vec{p}+\vec{q}}$ in Eq. (10) by one.

Pauli blocking, through the imaginary part of the Lindhard function, is the main nuclear effect included in the hadronic tensor of Eq. (10). In the next sections we will study additional nuclear corrections to $W^{\mu\nu}$.

A few words here on the low density theorem (LDT): when low nuclear density is supposed, the imaginary part of the Lindhard function can be approximated by a Dirac delta on energy (up to a constant factor) in such a way that the model reproduces the free space nucleon cross section.

## 4. Nuclear Model Corrections

### *4.1. Nuclear Correlations*

When the electroweak interactions take place in nuclei the strengths of electroweak couplings may change from their free nucleon values due to the presence of strongly interacting nucleons; indeed, since the nuclear experiments on $\beta$ decay in the early seventies [9], the quenching of axial current is a well established phenomenon. We follow here the many body approach of [1], and take into account the medium polarization effects in the 1p1h contribution to the $W^+$ boson self-energy by substituting it with an RPA response as shown diagrammatically in Fig. 3. For that purpose we use an effective ph–ph contact interaction

$$V = \; c_0 \left\{ f_0(\rho) + f_0'(\rho)\vec{\tau}_1\vec{\tau}_2 + g_0(\rho)\vec{\sigma}_1\vec{\sigma}_2 + g_0'(\rho)\vec{\sigma}_1\vec{\sigma}_2\vec{\tau}_1\vec{\tau}_2 \right\} \tag{11}$$

of the Landau-Migdal type. The density dependent coefficients were determined [10] from calculations of nuclear electric and magnetic moments, transition probabilities, and giant electric and magnetic multipole resonances. In the $S = T = 1$ channel ($\vec{\sigma}\vec{\sigma}\vec{\tau}\vec{\tau}$ operator) we use an interaction with explicit $\pi$ (longitudinal) and $\rho$ (transverse) exchanges, which has been used for the renormalization of the pionic and pion related channels in different nuclear reactions at intermediate energies [1, 5]. Further effects such as short range correlations (SRC) are also taken into account.

We also include $\Delta(1232)$ degrees of freedom in the nuclear medium which, given the spin-isospin quantum numbers of the $\Delta$ resonance, only modify the vector-isovector ($S = T = 1$) channel of the RPA response function.

The $V$ lines in Fig. 3 stand for the effective ph($\Delta$h)-ph($\Delta$h) interaction described so far. We should stress that this effective interaction is non-relativistic, and then for consistency we will neglect terms of order $\mathcal{O}(p^2/M^2)$ when summing

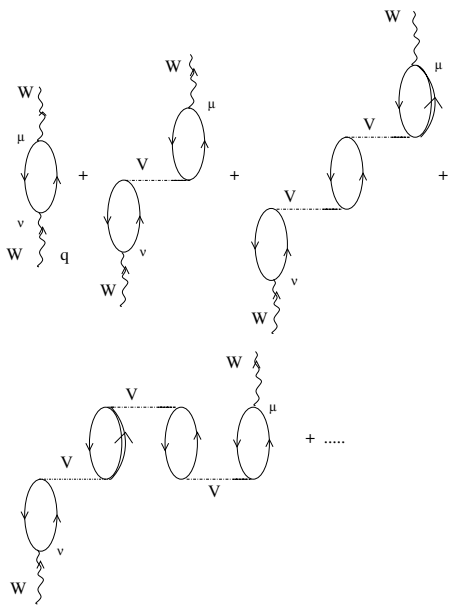


**Fig 3.** Set of irreducible diagrams responsible for the polarization (RPA) effects in the 1p1h contribution to the $W^+$ self-energy.

up the RPA series.

### *4.2. Energy Balance and Coulomb Distortion*

To ensure the correct energy balance in the reaction (1) for finite nuclei, the energy conserving Dirac delta function in Eq. (10) has to be modified by including the minimum excitation energy, $Q = M(A_{Z+1}) - M(A_Z)$, needed for the transition to the ground state of the final nucleus. The consideration of this energy gap is essential to obtain reasonable cross sections for low-energy neutrinos, see [11].

We also include a Coulomb self-energy $\Sigma_C = 2k'^0 V_C(r)$ in the intermediate lepton propagator of the neutrino self-energy depicted in Fig. 1 where $V_C(r)$ is the nucleus Coulomb potential produced by a charge distribution $\rho_{ch}(r)$. This way of taking into account the Coulomb effects has clear resemblances with what is called "modified effective momentum approximation" in [12].

### *4.3. FSI*

Once a ph excitation is produced by the virtual $W-$boson, the outgoing nucleon can collide many times, thus inducing the emission of other nucleons. The result is a quenching of the QE peak respect to the simple ph excitation calculation and a spreading of the strength, or widening of the peak. A distorted

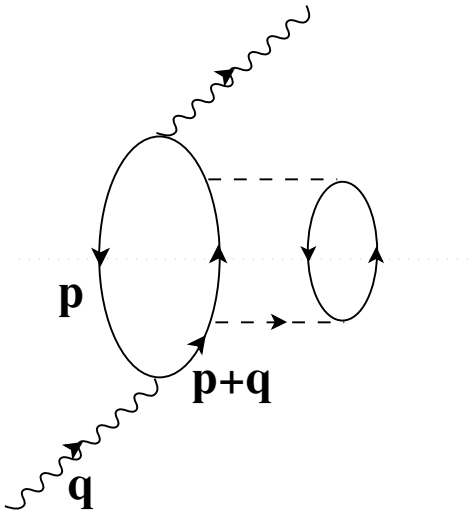


**Fig 4.** $W^+$ self-energy diagram obtained from the first diagram depicted in Fig. 2 by dressing up the nucleon propagator of the particle state in the ph excitation.

wave approximation with an optical (complex) nucleon-nucleus potential would remove all these events. However, if we want to evaluate the inclusive $(\nu_l, l^-)$ cross section these events should be kept and one must sum over all open final state channels.

We will account for the Final State Interaction (FSI) by using nucleon propagators properly dressed with a realistic self-energy in the medium, which depends explicitly on the energy and the momentum [13]. This self-energy has an imaginary part from the coupling to the 2p2h components, which is equivalent to the use of correlated wave functions, evaluated from realistic $NN$ forces and incorporating the effects of the nucleon force in the nucleon pairs. Thus, we consider the many body diagram depicted in Fig. 4.

Once we have got a model for the nucleon self-energy $\Sigma(p^0, \vec{p}; \rho)$, we can include in it a renormalized nucleon propagator $G_{\rm FSI}(p; \rho)$, that can be easily related to $S_p$ and $S_h$, the particle and hole spectral functions and then through

$$\mathrm{Im}\overline{U}_{FSI}(q; k_F) = -\frac{\Theta(q^0)}{4\pi^2} \int d^3p \int_{\mu-q^0}^{\mu} d\omega S_h(\omega, \vec{p}; \rho) S_p(q^0 + \omega, \vec{p} + \vec{q}; \rho) \qquad (12)$$

with the Lindhard function that we include in our formalism.

## 5. Low Energy Results

We present in Figs. 5 and 6 and Table 1 our theoretical predictions and a comparison with the experimental measurements of the inclusive $^{12}\mathrm{C}(\nu_\mu, \mu^-)X$

**Table 1.** Flux averaged $^{12}\mathrm{C}(\nu_e, e^-)X$ and $^{12}\mathrm{C}(\nu_\mu, \mu^-)X$ cross sections.

| | Theory | KARMEN [14] | LSND [15] | LAMPF [16] |
|---|---|---|---|---|
| $\overline{\sigma}_e$ | 0.14 | $0.15 \pm 0.01 \pm 0.01$ | $0.15 \pm 0.01 \pm 0.01$ | $0.141 \pm 0.023$ |
| | Theory | LSND'95 | LSND'97 | LSND'02 [17] |
| $\overline{\sigma}_\mu$ | 11.9 | $8.3 \pm 0.7 \pm 1.6$ | $11.2 \pm 0.3 \pm 1.8$ | $10.6 \pm 0.3 \pm 1.8$ |

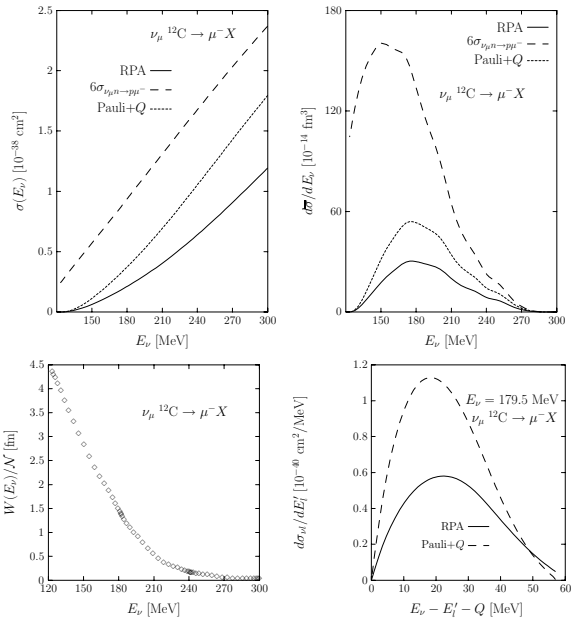


**Fig 5.** Predictions for the LSND experiment. See [8] for details.

and $^{12}\mathrm{C}(\nu_e, e^-)X$ reactions near threshold. Pauli blocking and the use of the correct energy balance improve the results, but only once RPA and Coulomb effects are included a good description of data is achieved.

Given the succes of the model at low energies we decided to further test it by calculating inclusive muon capture rates in nuclei throughout the Periodic Table. Results are given in Table 2 including the error in the theoretical predictions. Data were taken from [21], using a weighted average: $\overline{\Gamma}/\sigma^2 = \sum_i \Gamma_i/\sigma_i^2$, with $1/\sigma^2 = \sum_i 1/\sigma_i^2$.

Despite the huge range of variation of the capture widths, the agreement to data is quite good for all studied nuclei, with discrepancies of about 15% at most. Furthermore, using LFG instead of a more refined model such as a shell model does not affect much the value of integrated observables such as total cross

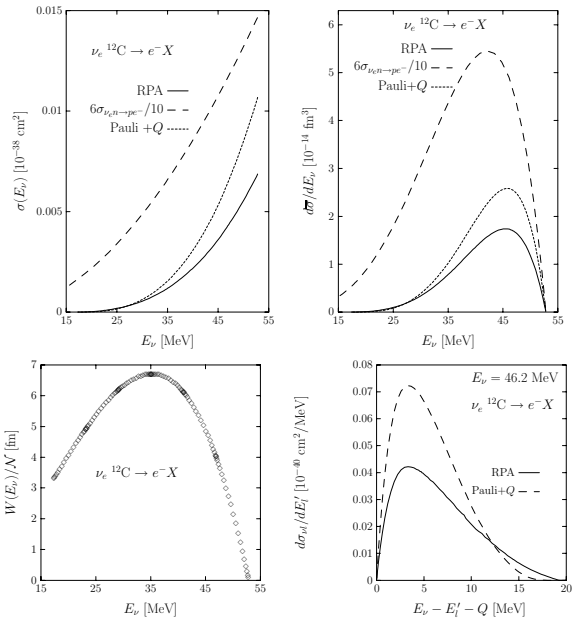


**Fig 6.** Predictions for the $^{12}\mathrm{C}(\nu_e, e^-)X$ reaction. See [8] for details.

**Table 2.** Experimental and theoretical total muon capture widths $\Gamma$, for different nuclei. See [8] for details.

| | Pauli+$\overline{Q}$ | RPA | Exp | $\left(\Gamma^{\mathrm{Exp}} - \Gamma^{\mathrm{Th}}\right)/\Gamma^{\mathrm{Exp}}$ |
|---|---|---|---|---|
| $^{12}$C | 5.42 | 3.21 | $3.78 \pm 0.03$ | 0.15 |
| $^{16}$O | 17.56 | 10.41 | $10.24 \pm 0.06$ | $-0.02$ |
| $^{18}$O | 11.94 | 7.77 | $8.80 \pm 0.15$ | 0.12 |
| $^{23}$Na | 58.38 | 35.03 | $37.73 \pm 0.14$ | 0.07 |
| $^{40}$Ca | 465.5 | 257.9 | $252.5 \pm 0.6$ | $-0.02$ |
| $^{44}$Ca | 318 | 189 | $179 \pm 4$ | $-0.06$ |
| $^{75}$As | 1148 | 679 | 609±4 | $-0.11$ |
| $^{112}$Cd | 1825 | 1078 | 1061±9 | $-0.02$ |
| $^{208}$Pb | 1939 | 1310 | 1311±8 | 0.00 |

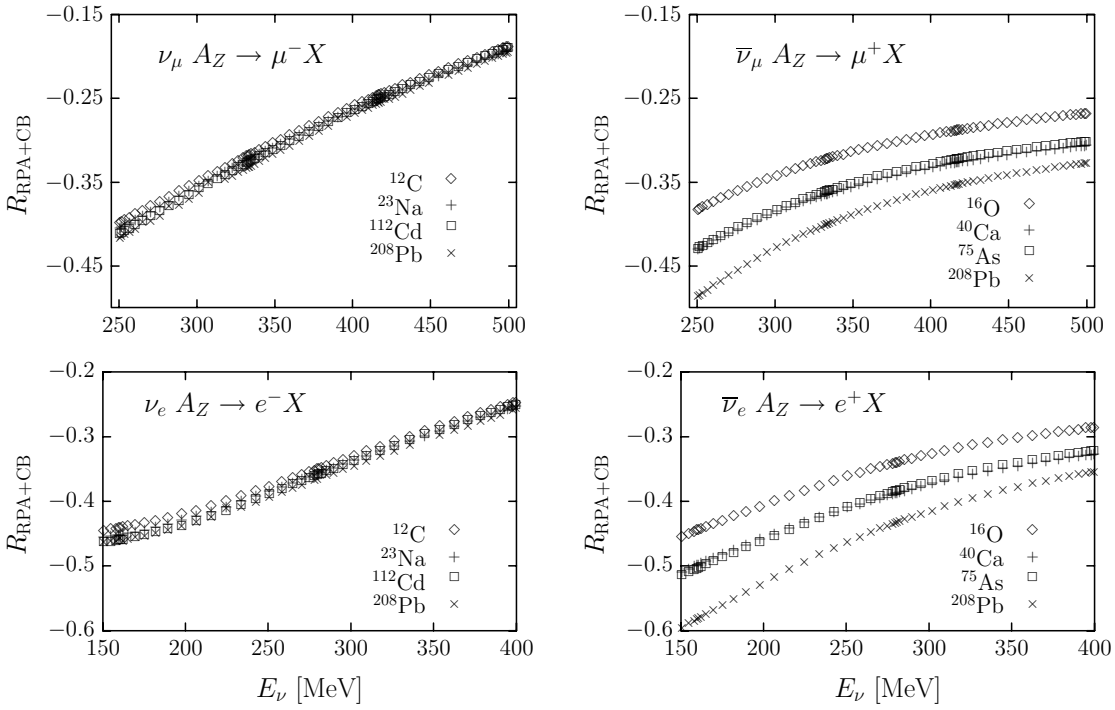


**Fig 7.** RPA and Coulomb (CB) corrections to electron and muon neutrino and antineutrino QE cross sections for different nuclei, as a function of the neutrino energy.

section or capture widths, see [23]. It is precisely for $^{12}$C where we find the greatest discrepancy with experiment. Nevertheless, our model provides one of the best existing combined description of the inclusive muon capture in $^{12}$C and the LSND measurement of the reaction $^{12}\mathrm{C}(\nu_\mu, \mu^-)X$ near threshold.

## 6. Intermediate Energy Results

At intermediate energies the predictions of this model should become reliable, not only for integrated, but also for differential cross sections. We present results for incoming neutrino energies within the interval 150-400 (250-500) MeV for electron (muon) species. The use of relativistic kinematics for the nucleons leads to moderate reductions in the interval of 4-9% for both neutrino and antineutrino cross sections, at the energies considered. Such corrections do not depend significantly on the considered nucleus.

In Fig. 7 the effects of RPA and Coulomb corrections are studied as a

**Table 3.** Muon and electron neutrino and antineutrino inclusive QE integrated cross sections from $^{16}$O.

| $E_\nu$ | | $\sigma\,(^{16}\mathrm{O}(\nu_\mu,\mu^-)X)$ | | | $\sigma\,(^{16}\mathrm{O}(\bar{\nu}_\mu,\mu^+)X)$ | | |
|---|---|---|---|---|---|---|---|
| | | REL | NOREL | FSI | REL | NOREL | FSI |
| 500 | Pauli | 460.0 | 497.0 | 431.6 | 155.8 | 168.4 | 149.9 |
| | RPA | 375.5 | 413.0 | 389.8 | 113.4 | 126.8 | 129.7 |
| 375 | Pauli | 334.6 | 354.8 | 292.2 | 115.1 | 122.6 | 105.0 |
| | RPA | 243.1 | 263.9 | 243.9 | 79.8 | 87.9 | 87.5 |
| 250 | Pauli | 155.7 | 162.2 | 122.5 | 63.4 | 66.4 | 52.8 |
| | RPA | 94.9 | 101.9 | 93.6 | 38.8 | 42.1 | 40.3 |

| $E_\nu$ | | $\sigma\,(^{16}\mathrm{O}(\nu_e,e^-)X)$ | | | $\sigma\,(^{16}\mathrm{O}(\bar{\nu}_e,e^+)X)$ | | |
|---|---|---|---|---|---|---|---|
| | | REL | NOREL | FSI | REL | NOREL | FSI |
| 310 | Pauli | 281.4 | 297.4 | 240.6 | 98.1 | 104.0 | 87.2 |
| | RPA | 192.2 | 209.0 | 195.2 | 65.9 | 72.4 | 73.0 |
| 220 | Pauli | 149.5 | 156.2 | 121.2 | 60.7 | 63.6 | 51.0 |
| | RPA | 90.1 | 97.3 | 92.8 | 36.8 | 40.0 | 40.2 |
| 130 | Pauli | 37.0 | 38.3 | 28.8 | 21.1 | 21.9 | 16.9 |
| | RPA | 20.6 | 22.3 | 23.3 | 10.9 | 11.9 | 12.8 |

function of the incoming neutrino/antineutrino energy. The correction $R_{\mathrm{RPA+CB}}$ is defined as $(\sigma_{\mathrm{RPA+CB}} - \sigma_0)/\sigma_0$, where $\sigma_0$ does not include RPA and Coulomb corrections, while $\sigma_{\mathrm{RPA+CB}}$ includes these nuclear effects. FSI corrections are not taken into account in these cross sections. RPA correlations reduce the cross sections, and we see large effects, specially at lower energies. Nevertheless, for the highest energies considered (500 and 400 MeV for muon and electron neutrino reactions, respectively) we still find suppressions of about 20-30%. Coulomb distortion of the outgoing charged lepton enhances (reduces) the cross sections for neutrino (antineutrino) processes and its effects decrease with energy. For antineutrino reactions, the combined effect of RPA and Coulomb corrections have a moderated dependence on $A$ and $Z$. At the high energy end the $A-$dependence becomes milder, since Coulomb distortion becomes less important. In the case of neutrinos, the increase of the cross section due to Coulomb cancels out partially with the RPA reduction. Finally, the existing differences between electron and muon neutrino/antineutrino plots are due to the different momenta of an electron and a muon with the same energy.

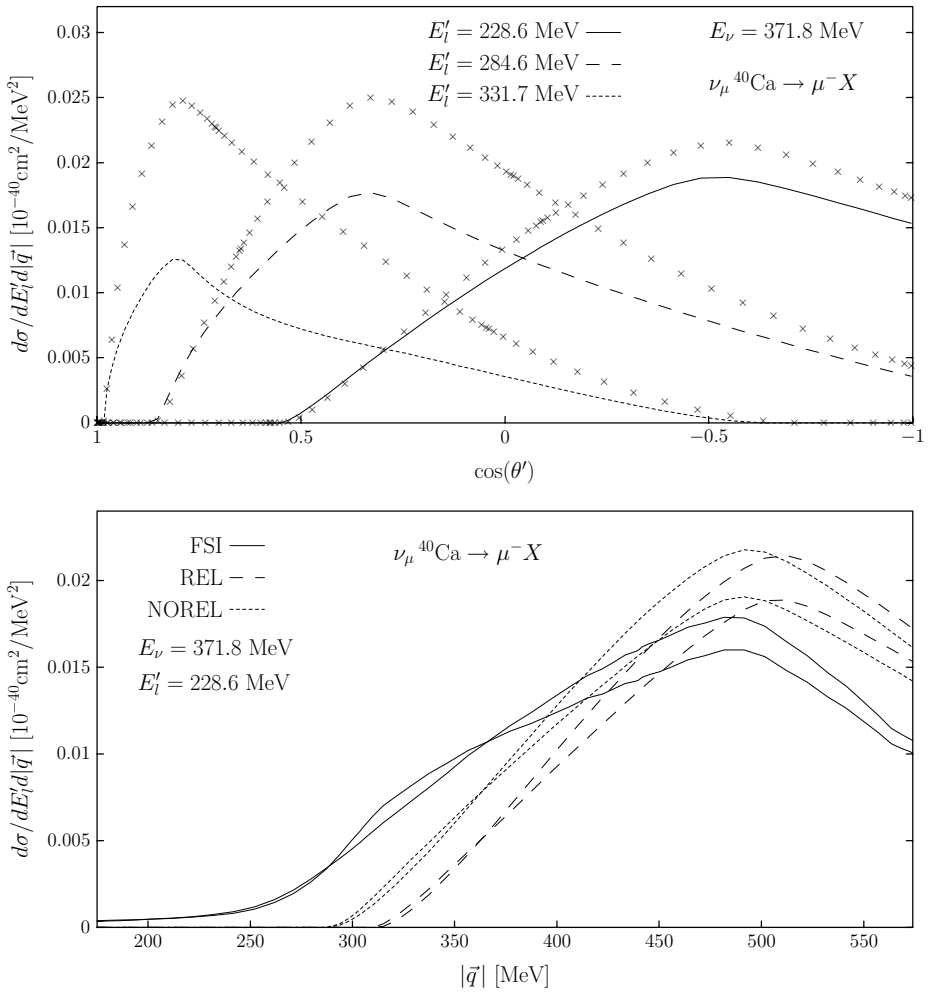


**Fig 8.** Muon neutrino differential cross sections in calcium as a function of the lepton scattering angle (top) and of the momentum transfer (bottom). **Top**: Cross sections, without FSI and using relativistic kinematics for the nucleons. Crosses have been obtained without RPA and Coulomb effects, while the curves have been obtained with the full model (up to FSI effects). **Bottom**: Cross sections, obtained by using relativistic (REL) and non-relativistic nucleon kinematics results with (FSI) and without (NOREL) FSI effects. We also take into account RPA and Coulomb corrections (lower lines at the peak).

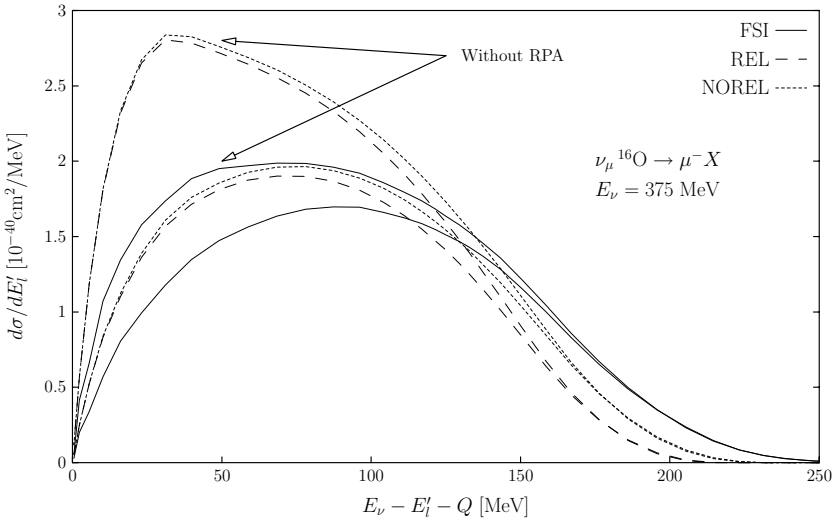


**Fig 9.** Muon neutrino QE differential cross sections in $^{16}$O as a function of the energy transfer. We show results for relativistic (long dashed line, 'REL') and non-relativistic nucleon kinematics with (solid line, 'FSI') and without (short dashed line, 'NOREL') FSI effects. We also show the effect of RPA and Coulomb corrections (lower lines at the peak).

In Figs. 8 and 9 FSI effects on differential cross sections are shown. As expected, FSI provides a broadening and a significant reduction of the strength of the QE peak. Finally, in Table 3 we compile muon and electron neutrino and antineutrino inclusive QE integrated cross sections from oxygen. We present results for relativistic (REL) and non-relativistic nucleon kinematics and in this latter case, we present results with (FSI) and without FSI (NO-REL) effects. Though FSI changes importantly the shape of the differential cross sections, it plays a minor role when one considers total cross sections. When medium polarization effects are not considered, FSI provides significant reductions (13-29%) of the cross sections [22]. However, when RPA corrections are included, the reductions becomes more moderate, always smaller than 7%; even there exist some cases where FSI enhances the cross sections. This can be easily understood by looking at Fig. 9 where we show the differential cross section as a function of the energy transfer for $E_\nu = 375$ MeV. There, we see that FSI increases the cross section for high energy transfer. But for nuclear excitation energies higher than those around the QE peak, the RPA corrections are certainly less important than in the peak region. Hence, the RPA suppression of the FSI distribution is significantly smaller than the RPA reduction of the distribution determined by the ordinary Lindhard

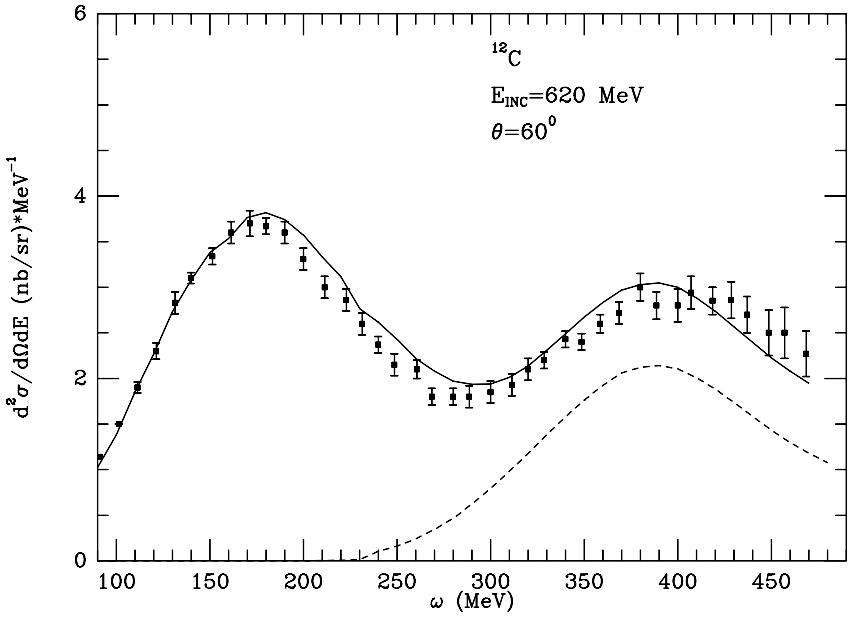


**Fig 10.** Double differential $^{12}\mathrm{C}(e,e')X$ cross section

function.

## 7. Previous results

The same formalism presented here has been used in previous works studying real [5] and virtual [1] photon inclusive nuclear reactions. Excellent results both in the quasielastic and $\Delta$ excitation regions where obtained in these works. To describe the $\Delta$ peak and the "dip" regions, they included a high number of gauge boson absorption modes so they were able to study the reaction at higher nuclear excitation energies than those we have presented here. As can be seen for instance in Fig. 10 the agreement with experiment is excellent. Furthermore, inclusive processes of the type $(e,e'N)$, $(e,e'NN)$, $(e,e'\pi)$ were studied by means of a MonteCarlo simulation as presented in [24] that make use of the nuclear and pion physics models of [6] and [7]. It is because of the remarkable succes of this model that we expect our work to be highly reliable for CC reactions.

## 8. Conclusion and Outlook

We have presented here a many body approach to inclusive electroweak reactions in nuclei, at intermediate energies (nuclear excitation energies below 500 MeV). It systematically takes into account RPA, SRC, $\Delta(1232)$, FSI and MEC effects. The meson-nucleon and nucleon-nucleon dynamics of the approach have

been successfully tested in former pionic reactions.

It has been tested succesfully in:

- Real and virtual photo-absorption and $\pi$, $N$, $NN$, $N\pi$ electro and photo-production processes in nuclei.
- Charged current induced inclusive neutrino $^{12}\mathrm{C}(\nu_\mu, \mu^-)X$ cross sections at low energies and Inclusive Muon capture in Nuclei.

Predictions for QE neutrino induced reactions in nuclei at intermediate energies of interest for future neutrino experiments have been presented.

Our intention is to improve this approach by including contributions from resonance degrees of freedom and MEC in the charged current reactions. We also want to extend this formalism to exclusive channels in neutral currents via a MonteCarlo simulation.

## 9. List of Symbols/Nomenclature

We have used $\hbar = c = 1$ units for formulas all throughout this work, however results in tables and figures are presented in the following units unless otherwise noted.

| | |
|---|---|
| $\vec{k}$ = LAB lepton momenta, MeV | $E_{\vec{p}}$ = Energy of $p$ momentum lepton, MeV |
| $\rho$ = Nuclear matter density | $\sigma$ = Cross section, $10^{-40}\mathrm{cm}^2$ |
| $\vec{\sigma}$ = Spin Pauli matrices | $\vec{\tau}$ = Isospin Pauli matrices |
| $k_F^n$ = Fermi momentum for neutrons | $k_F^p$ = Fermi momentum for protons |
| $q$ = Transfered $W$ momentum | $\Gamma$ = Muon capture widht, $10^{-4}\mathrm{s}^{-1}$ |
| $\Theta(x)$ = Step function | |

## References


[1] A. Gil, J. Nieves and E. Oset, Nucl. Phys. A 627 (1997) 543.

[2] T. Kajita and Y. Kotsuka, Rev. of Mod. Phys. 73 (2001) 85.

[3] Proceedings of the RCCN International Workshop on *Sub-Dominant Oscillations Effects in Atmospheric Neutrino Experiments* (2005) Universal Academy Press, Tokyo.

[4] Y. Fukuda *et al.*, Phys. Lett. B 433 (1998) 9.

[5] R. Carrasco and E. Oset, Nucl. Phys. A 536 (1992) 445.

[6] E. Oset, H. Toki and W. Weise, Phys. Rep. 83 (1982) 281.

[7] J. Nieves, E. Oset, C. García-Recio, Nucl. Phys. A 554 (1993) 509; *ibidem*, Nucl. Phys. A554 (1993) 554; E. Oset *et al.*, Prog. Theor. Phys. Suppl. 117

(1994) 461; C. Albertus, J. E. Amaro and J. Nieves, Phys. Rev. Lett. 89 (2002) 032501; *ibidem*, Phys. Rev. C 67 (2003) 034604.
[8] J. Nieves, J. E. Amaro and M. Valverde, Phys. Rev. C 70 (2004) 055503.
[9] D. H. Wilkinson, Nucl. Phys. A 209 (1973) 470, A 225 (1974) 365.
[10] J. Speth, E. Werner and W. Wild, Phys. Rep. 33 (1977) 127; J. Speth, V. Klemt, J. Wambach and G. E. Brown, Nucl. Phys. A 342 (1980) 382.
[11] N. C. Mukhopadhyay *et al.*, Phys. Lett. B 434 (1998) 7.
[12] J. Engel, Phys. Rev. C 57 (1998) 2004.
[13] P. Fernández de Córdoba and E. Oset, Phys. Rev. C 46 (1992) 1697.
[14] B. Zeitnitz, Prog. Part. Nucl. Phys. 32 (1994) 351; B. E. Bodmann *et al.*, Phys. Lett. B 332 (1994) 251.
[15] M. Albert *et al.*, Phys. Rev. C 51 (1995) 1065; C. Athanassopoulos *et al.*, Phys. Rev. C 56 (1997) 2806; L. B. Auerbach *et al.*, Phys. Rev. C 66 (2002) 015501.
[16] D. A. Krakauer *et al.*, Phys. Rev. C 45 (1992) 2450.
[17] C. Athanassopoulos, *et al.*, Phys. Rev. C 55 (1997) 2078.
[18] A. C. Hayes and I. S. Towner, Phys. Rev. C 61 (2000) 044603.
[19] C. Volpe *et al.*, Phys. Rev. C 62 (2000) 015501.
[20] E. Kolbe, K. Langanke, G. Martínez-Pinedo and P. Vogel, J. Phys. G 29 (2003) 2569.
[21] T. Suzuki, D. F. Measday and J. P. Roalsvig, Phys. Rev. C 35 (1987) 2212 and references therein.
[22] C. Maieron, M. C. Martinez, J. A. Caballero and J. M. Udias, Phys. Rev. C 68 (2003) 048501.
[23] J. E. Amaro, C. Maieron, J. Nieves and M. Valverde, nucl-th/ 0409017.
[24] A. Gil, E. Oset and J. Nieves, Nucl. Phys. A 627 (1997) 599.